Sea Exploitation and Environment 2024, 1:2
International R&D Publishing www.irdpub.com

Research

Predictions of Sloshing Height Induced by Seismic Excitations Based on LSTM

Yi-Yi Qin[1], Zhi-Yu Wang[1], Yu-Sheng Wang[1,*], Fu-Gui Zhang[1,2], Xin, Jin[1,2]

1 College of Electronic Engineering, Chengdu University of Information Technology, Chengdu 610225, China

2 CMA. Key Laboratory of Atmosphere Sounding, Chengdu University of Information Technology, Chengdu 610225, China

Keywords:

Recurrent Neural Network;
LSTM;
Sloshing height;
Seismic excitation

Cited as:
Qin Y., Wang, Z., Wang, Y., Zhang, F., Jin, X. Predictions of Sloshing Height Induced by Seismic Excitations Based on LSTM. Sea Exploitation and Environment, (2024) 1:2.
https://doi.org/10.62813/sea.2024.01.03

Abstract:

Present work aims to predict the sloshing height induced by seismic excitations by the Long-Short Term Memory (LSTM), which is a temporal recurrent neural network and has the time connection ability to reconstruct the main features of nonstationary records. Lushan and California earthquakes are selected as the external excitations, and thus yield two groups of time-series free surface elevations as the training samples. The internal structural parameters of LSTM, such as epochs, batch size, and input shape, are systematically adjusted. The errors and correlations between the predicted and actual results are also analyzed. The input step is set as 50, and the proportion of the training set is 80%. The results show that the errors are respectively lower than 0.3% and 2.0%, and the correlations reach 0.998 for both cases. Overall, LSTM can well predict the sloshing heights because of the advantage of predicting the long sequential data.

1. Introduction

Liquid sloshing induced by seismic excitations is a natural phenomenon which would threaten the safety of people or contaminate the environment (Goudarzi et al., 2010; Jin et al., 2021; Shao et al., 2012). To reveal the nature of this problem, most researchers adopted the numerical models based on Navier-Stokes equations. Dincer et al. studied the effects of near-fault seismic excitations on the sloshing wave and elastic structure based on the coupling method of smoothed particle hydrodynamics (SPH) and finite element method (FEM) (Dincer, 2019). Eswaran et al. numerically studied liquid sloshing in the Fuel Storage Bay (FSB) of advanced reactors under seismic loads (Eswaran and Reddy, 2016). Chen et al. simulated the three-dimensional nonlinear sloshing problem based on the Boundary Element Method (BEM) and analyzed liquid sloshing in cylindrical and rectangular storage tanks subjected to both harmonic and seismic excitations (Chen et al., 2007). It should be emphasized that the computational efficiency of those models is low (Hashimoto et al., 2017; Dincer, 2019). Therefore, there is a necessity to find a reliable and efficient alternative to reconstruct liquid sloshing induced by seismic excitations.

With the development of Machine Learning (ML), the surrogate models, for example, Multi-Layer Perceptron (MLP) (Taud and Mas, 2018), Backward Propagation (BP) (Li et al., 2012), Recurrent Neural Network (RNN), and Long-Short Term Memory (LSTM) (Sherstinsky, 2020; Manaswi, 2018), based on Artificial Neural Network (ANN) (Benbrahim et al., 2007), are developed and applied to study the hydrodynamics problems. Compared to other models, LSTM can capture nonlinear patterns in the long time-series data, and meantime fully considers time dependences (Wang et al., 2017; Abbasimehr et al., 2020). Wang et al. introduced a LSTM system, which combines the cross-correlation and association rules (Apriori), to study the characteristics of river pollutants and trace the industrial point source (Wang et al., 2017). The results show that LSTM can precisely predict the flow process of the pollutants. Fan et al. realized a quick prediction of the effective wave height based on LSTM (Fan et al., 2020). The results demonstrate that LSTM is superior to other algorithms, for example, extreme Learning Machine (ELM) and Support Vector Machine (SVM) algorithms. Shi et al. proposed a Multi-Input Long-Short Term Memory (MILSTM) neural network to predict the motion response of floating offshore wind turbine platforms (Shi et al., 2023), and concluded that MILSTM is suitable for studying the second-order problems. The above works demonstrate a promising application of

*Corresponding author.
E-mail address: 2643154716@qq.com (Yu-Sheng Wang).

Received September 6, 2023; revised December 19, 2023; accepted December 29, 2024; available online September 11, 2024.

LSTM in the hydrodynamics problems.

Considering the advantages of LSTM in predicting hydrodynamics problems, we adopt it to predict the sloshing height induced by seismic excitations. The Lushan and California earthquakes are selected as external seismic excitations to generate two groups of training samples, namely the sloshing heights. Firstly, two samples are analyzed and their basic regularity is revealed. Next, the principle and architecture of LSTM are introduced and explained in detail. Then, LSTM is employed to predict the sloshing height, and the errors and correlations are analyzed. Finally, the conclusion is presented in the last section.

2. Methods

2.1. Input samples

Two seismic excitations, namely Lushan at 51BXD station (2013) (Case 1) and California at Cape Mendocino station (1992) (Case 2) are chosen as the external excitations. A two-dimensional (2-d) rectangular tank with length L = 20 m, still water depth h = 12 m is used. The ground accelerations of Case 1 and Case 2 are demonstrated in Fig. 1. From this figure, Case 1 exhibits a lower Peak Ground Acceleration (PGA) with respect to Case 2. It is worth noting that although both cases are strong earthquakes with almost identical magnitudes (respectively 7.0 g and 7.1 g for Case 1 and Case 2, where g = 9.81 m/s2); the Peak Ground Velocity (PGV) of Case 1 is significantly lower than that of Case 2, respectively being 0.245 m/s and 1.26 m/s. This suggests that Case 2 has stronger seismic intensity compared to Case 1.

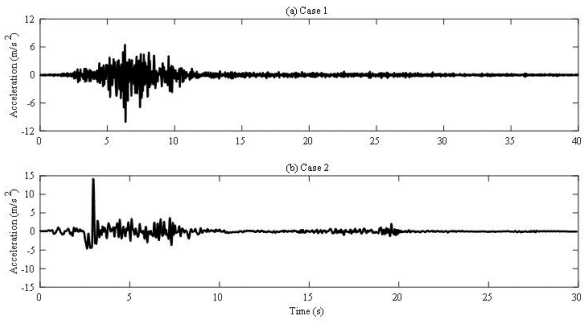

Fig. 1. Time histories of ground accelerations of two cases.

The numerical generated waves from a Navier-Stokes solver with a sampling frequency of 100 Hz are exampled in Fig. 2. From this figure, the data at the initial period (the first 4 s of Fig. 2(a) and the first 2.5 s of Fig. 2(b)) are faint. As time evolves, the ground acceleration gradually increases, suggesting more energy being input to the water bulk, and thus conspicuous free surface elevations are obtained. However, the regularity is still not sufficiently pronounced at this stage (4 s to 11 s in Fig. 2(a) and 2.5 s to 6 s in Fig. 2(b)). After this stage, the sloshing wave enters the steady state, and behaves as a sinusoidal function.

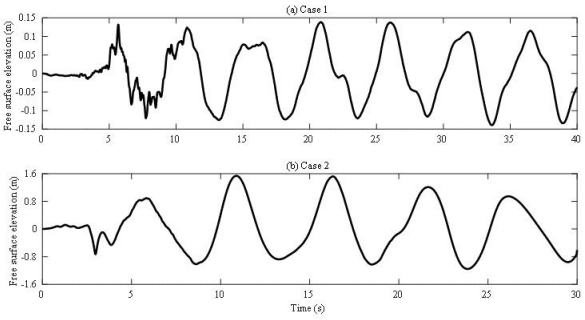

Fig. 2. Time histories of free surface elevations of two cases.

2.2. LSTM method

LSTM is a representative method in ANN that can bring in the time connection function to explore the dependencies and characteristics of the long time-series data (Siami-Namini et al., 2018). It utilizes the hidden layer as a memory unit to establish connections between current and previous inputs, which can simultaneously comprehend the current state and capture crucial information of the past state (Zhao et al., 2017). It should be emphasized that the input order significantly affects the training results. Additionally, it is designed to efficiently extract features from data while simultaneously avoiding the common issue of overfitting.

Fig.3 displays the flow diagram of LSTM. It needs to pass three gates, namely forgetting, input, and output. Firstly, the forgetting gate serves the purpose of determining whether to forget the input information from the previous node. Secondly, the information is selectively memorized by the input gate. To get the new state, the hyperbolic tangent function (tanh) shown in Eq. (1) is used to normalize and integrate the new input information. Finally, the output is determined by convolving the signal of the output gate to obtain the one step size (Hasegawa et al., 2020).

$$\tanh(x) = \frac{e^{x} - e^{-x}}{e^{x} + e^{-x}} \tag{1}$$

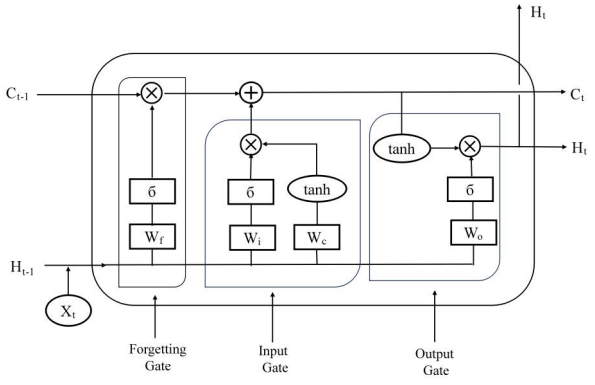

Fig. 3. The flow diagram of LSTM.

2.3. Construction of LSTM model

The Keras library in TensorFlow is employed in constructing the LSTM model. Before designing the model structure, an input step of 50 is adopted in the present model (Meng et al., 2022). The model consists of one input layer, three hidden layers each with 128 neurons, and one output layer. To prevent over-fitting, a Dropout layer (set as 0.2) is incorporated after each hidden layer. Furthermore, four hyper-parameters need to be set, including the loss function (set as Mean Square Error), algorithm of optimization (set as Adam), batch size (set as 32) and epochs (set as 50). Following these principles, the detailed structure of the LSTM model is illustrated in Fig. 4.

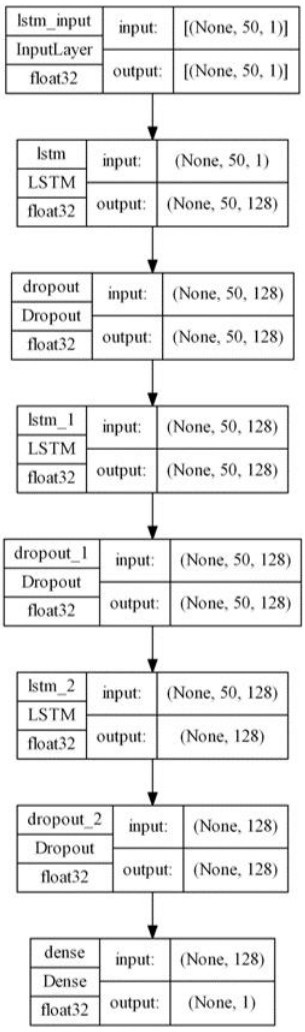

Fig. 4. The structure of the LSTM model.

3 Results and Discussion

3.1. Forecasting sloshing height

Generally, the sample data is divided into two parts: the training set and the test set, which are used to update the model parameters and evaluate the model's generalizability, respectively. The proportion of training samples is suggested 70% to 90% (Halder et al., 2023; Luo et al., 2023; Liu et al., 2022). Here, we take the median value of 80% as the training set and the remaining as the test set. The declining curves of loss function for Case 1 and Case 2 are presented in Fig. 5. From this figure, both decline noticeably to approximately 0.002 till the epochs are less than 5, and for larger epochs, only a slow fluctuation less than 0.002 appears.

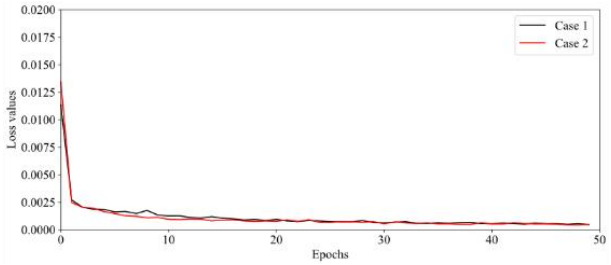

Fig. 5. Declining curves of Loss function of two cases.

The comparisons of the free surface elevations in the test set between the predicted and actual are shown in Fig. 6. It is evident that the predicted of Case 1 and Case 2 are consistent with the actual, highlighting the prediction ability of the LSTM model. Relatively larger but also faint errors are distributed within 35.5 s to 37 s in Fig. 6(a) and 25.6 s to 27.4 s in Fig. 6(b). Generally, when the nonlinearity (larger peak and lower trough) of data grows, the model accuracy decreases (Seydoux et al., 2020). For example, better agreement between the predicted and actual is reached except several time durations, for example, 33.6s to 33.9s, 36.0s to 36.5s and 38.8s to 39.2s in Fig. 6(a), and 29.5s to 30.0s in Fig. 6(b) (such as 33.7 s, 36.5 s, and 38.8 s in Fig. 6 (a), 26 s, and 29.5 s in Fig. 6(b). Overall, the superior predictive effects of Case 1 over Case 2 can be attributed to the fact that the sample capacity of Case 1 is larger than that of Case 2. Consequently, the model can learn sufficient information to better fit the training samples.

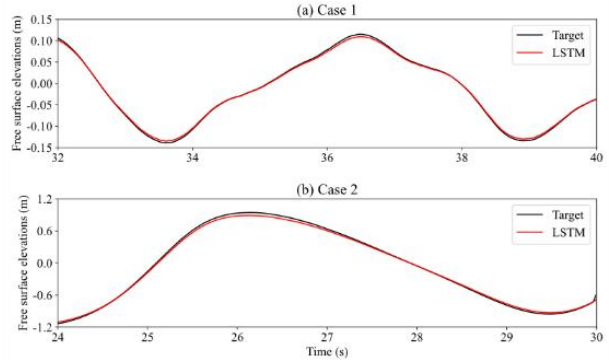

Fig. 6. Comparisons of time-history free surface elevations between the predicted by LSTM and actual in the test set of two cases.

3.2. Errors and Correlations

To quantify the prediction effects intuitively, we analyze

errors and correlations between the predicted and actual. Two indices, Absolute Error (AE) and Root Mean Square Error (RMSE), are used to measure the errors, and Correlation Coefficient (R^2) is adopted to evaluate their correlations (Xie et al., 2022). The formulas of AE, RMSE, and R^2 are respectively shown in Eqs. (2) – (4), as follows:

$$\mathrm{AE} = \left| x_i - x_i^* \right| \tag{2}$$

$$\mathrm{RMSE} = \sqrt{\frac{\sum_{i=1}^{n} (x_i - x_i^*)^2}{n}} \tag{3}$$

$$R^2 = 1 - \frac{\sum_{i=1}^{n} (x_i - x_i^*)^2}{\sum_{i=1}^{n} (x_i - x)^2} \tag{4}$$

where x_i and x_i^* are the ground truth and predicted value of the ith sample, respectively, x is the average of the ground truths, and n is the number of samples. For AE and RMSE, a lower value indicates higher accuracy, whereas a larger R^2 value signifies a stronger correlation.

The AE of the predicted and actual in the test set are depicted in Fig. 7. It follows that all cases exhibit small AE values, implying the reliability of the LSTM model to produce a satisfactory prediction. Besides, Case 1 exhibits smaller AE values than that of Case 2. This illustrates that Case 1 presents better prediction performance over Case 2. The large values of AE typically appear at extreme points of the free surface elevations. After these extreme points, the values likewise decrease accordingly, from 0.005 to 0.001. Significantly, at the last time of Case 2 (nearly 30 s), the values of AE increase sharply over 0.1 due to violent rise in free surface elevations and substantial nonlinearity.

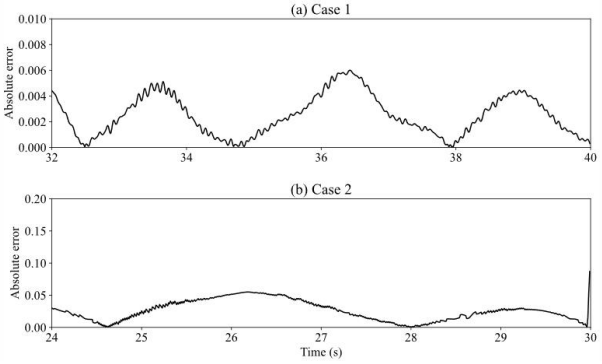

Fig. 7. The AE of time histories in the test set of two cases.

The comparisons of the RMSE values between the predicted and actual in the training and test sets are demonstrated in the left column of Fig. 8. The RMSE values of Case 1 and Case 2 are respectively 0.0028 and 0.0178 in the training set and 0.0027 and 0.0196 in the test set. It can be seen that the RMSE of all samples is small, indicating the numerical results agree well with the actual. The maximum and minimum values of RMSE are respectively 0.0196 and 0.0027. The RMSE values of the training and test sets are close, meaning the model can accurately fit samples outside the training set. Clearly, the RMSE value of Case 1 is lower than that of Case 2, and the reason for this discrepancy might be that the sample capacity of Case 1 is larger than that of Case 2. Moreover, the nonlinear strength of data is also an important factor influencing the predicted accuracy. By comparisons, the asymmetry of the equilibrium position of Case 2 is more obvious than Case 1, meaning Case 2 exhibits weaker linearity than Case 1, which further confirms that the prediction effects of Case 1 are superior to Case 2 is reasonable.

The comparisons of the R^2 values between the predicted and actual are quantified in the right column of Fig. 8. The R^2 values of Case 1 and Case 2 are respectively 0.9990 and 0.9988 in the training set and 0.9992 and 0.9983 in the test set. Besides, the R^2 of all samples exceed 0.998. This indicates that the overall prediction accuracy is pretty good.

In conclusion, it can be deduced that LSTM, a surrogate model, possesses excellent prediction capability especially for sample sets with strong linearity or large capacity, and proves that it is suitable to predict the free surface elevations. In practical scenarios, the prediction accuracy can be improved by adjusting the model parameters.

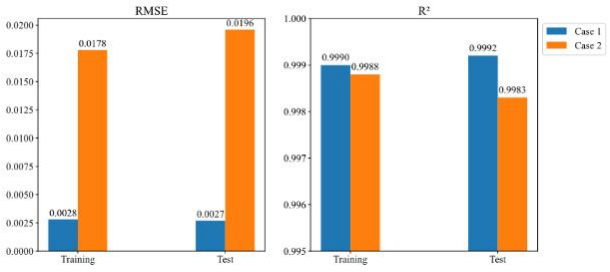

Fig. 8. Temporal averaged RMSE (left column) and R^2 (right column) in the training and test sets of two cases.

4. Conclusions

A LSTM-based prediction of free surface elevations induced by seismic excitations is realized in this paper. This result indicates that LSTM can accurately capture the characteristics of free surface elevations and exhibits the potential to predict nonlinear and complex data sequences. Although there are slight deviations between the predicted and actual, the result implies that the overall prediction accuracy is pretty good, which preliminarily shows the practicality of utilizing LSTM for the prediction of free

surface elevations.

The prediction accuracy is significantly impacted by sample capacity and data nonlinearity. Compared to Case 2 with a smaller capacity, Case 1 performs even better. The RMSE of Case 2 exceeds 1.7%, while that of Case 1 is less than 0.3%. This is because stronger nonlinearity of Case 2.

In a word, the LSTM is an economical and efficient method to precisely predict the liquid sloshing. Future work will be focused on the long-duration predictions of the three-dimensional free surface and flow field.

Author contribution statement

Yi-Yi Qin: Writing-original draft, Investigation, Formal analysis, Data curation. **Zhi-Yu Wang**: Conceptualization, Methodology, Writing-review & editing. **Yu-Sheng Wang**: Conceptualization, Methodology, Supervision, Writing-review & editing, Funding acquisition. **Fu-Gui Zhang**: Writing-review & editing. **Xin Jin**: Investigation, Data curation, Writing-review & editing.

Declaration of competing interest

The authors declare no known competing interests that could influence the work reported in this paper.

Acknowledgements

The work was supported, in part, by the Key R&D program of Science & Technology Department of Sichuan Province (Grant No. 2024YFHZ0173).

References

Goudarzi M. A., Sabbagh-Yazdi S. R., Marx W. Seismic analysis of hydrodynamic sloshing force on storage tank roofs[J]. Earthquake Spectra, 2010, 26(1), 131–152.

Jin X., Xue M. A., Lin P. Z. Numerical modeling and formulation of the runup of seismically-induced surge waves in idealized reservoirs[J]. Soil Dynamics and Earthquake Engineering, 2021, 143, 106625.

Shao J. R., Li H. Q., Liu G. R., et al. An improved SPH method for modeling liquid sloshing dynamics[J]. Computers & Structures, 2012, 100, 18–26.

Dincer A. E. Investigation of the sloshing behavior due to seismic excitations considering the two-way coupling of the fluid and the structure[J]. Water, 2019, 11(12), 2664.

Eswaran M., Reddy G. R. Liquid sloshing in fuel storage bays of advanced reactor subjected to earthquake loading[J]. Procedia Engineering, 2016, 144, 1278–1285.

Chen Y. H., Hwang W. S., Ko C. H. Sloshing behaviours of rectangular and cylindrical liquid tanks subjected to harmonic and seismic excitations[J]. Earthquake Engineering & Structural Dynamics, 2007, 36(12), 1701–1717.

Hashimoto H., Hata Y., Kawamura K. Estimation of oil overflow due to sloshing from oil storage tanks subjected to a possible Nankai Trough earthquake in Osaka Bay area[J]. Journal of Loss Prevention in the Process Industries, 2017, 50, 337–346.

Dincer A. E. Investigation of the sloshing behavior due to seismic excitations considering two-way coupling of the fluid and the structure[J]. Water, 2019, 11(12), 2664.

Benbrahim M., Daoudi A., Benjelloun K., et al. Discrimination of seismic signals using artificial neural networks[J]. International Journal of Computer and Information Engineering, 2007, 1(4), 984–987.

Taud H., Mas J. F. Multilayer perceptron (MLP)[J]. Geomatic Approaches for Modeling Land Change Scenarios, 2018, 451–455.

Li J., Cheng J., Shi J., et al. Brief introduction of back propagation (BP) neural network algorithm and its improvement[C]. Advances in Computer Science and Information Engineering: Volume 2, Springer Berlin Heidelberg, 2012, 553–558.

Sherstinsky A. Fundamentals of recurrent neural network (RNN) and long short-term memory (LSTM) network[J]. Physica D: Nonlinear Phenomena, 2020, 404, 132306.

Manaswi N. K. RNN and LSTM[J]. Deep learning with Applications Using Python, 2018, 115-126.

Wang Q., Guo Y., Yu L., et al. Earthquake prediction based on spatio-temporal data mining: an LSTM network approach[J]. IEEE Transactions on Emerging Topics in Computing, 2017, 8(1), 148–158.

Abbasimehr H., Shabani M., Yousefi M. An optimized model using LSTM network for demand forecasting[J]. Computers & Industrial Engineering, 2020, 143, 106435.

Wang P., Yao J., Wang G., et al. Exploring the application of artificial intelligence technology for identification of water pollution characteristics and tracing the source of water quality pollutants[J]. Science of the Total Environment, 2019, 693, 133440.

Fan S., Xiao N., Dong S. A novel model to predict significant wave height based on long short-term memory network[J]. Ocean Engineering, 2020, 205, 107298.

Shi W., Hu L., Lin Z., et al. Short-term motion prediction of floating offshore wind turbine based on multi-input LSTM neural network[J]. Ocean Engineering, 2023, 280, 114558.

Siami-Namini S., Tavakoli N., Namin A. S. A comparison of ARIMA and LSTM in forecasting time series[C]. Proceedings of the 17th IEEE International Conference on Machine Learning and Applications (ICMLA), IEEE, 2018, 1394–1401.

Zhao Z., Chen W., Wu X., et al. LSTM network: a deep learning approach for short-term traffic forecast[J]. IET Intelligent Transport Systems, 2017, 11(2), 68–75.

Shewalkar A., Nyavanandi D., Ludwig S. A. Performance evaluation of deep neural networks applied to speech recognition: RNN, LSTM and GRU[J]. Journal of Artificial Intelligence and Soft Computing Research, 2019, 9(4), 235–245.

Hasegawa K., Fukami K., Murata T., et al. Machine-learning-based reduced-order modeling for unsteady flows around bluff bodies

of various shapes[J]. Theoretical and Computational Fluid Dynamics, 2020, 34(4), 367–383.

Meng Z. F., Chen Z., Khoo B. C., et al. Long-time prediction of sea wave trains by LSTM machine learning method[J]. Ocean Engineering, 2022, 262, 112213.

Halder R., Damodaran M., Khoo B. C. Deep learning-driven nonlinear reduced-order models for predicting wave–structure interaction[J]. Ocean Engineering, 2023, 280, 114511.

Luo X., Kareem A., Yu L., et al. A machine learning-based characterization framework for parametric representation of liquid sloshing[J]. Results in Engineering, 2023, 18, 101148.

Liu Y., Hu R., Kraus A., et al. Data-driven modeling of coarse mesh turbulence for reactor transient analysis using convolutional recurrent neural networks[J]. Nuclear Engineering and Design, 2022, 390, 111716.

Seydoux L., Balestriero R., Poli P., et al. Clustering earthquake signals and background noises in continuous seismic data with unsupervised deep learning[J]. Nature Communications, 2020, 11(1).

Xie C., Liu X. D., Man T. H., et al. PWPNet: A deep learning framework for real-time prediction of significant wave height distribution in a port[J]. Journal of Marine Science and Engineering, 2022, 10(10), 1375.